Journal of Materials Chemistry A

Accepted Manuscript

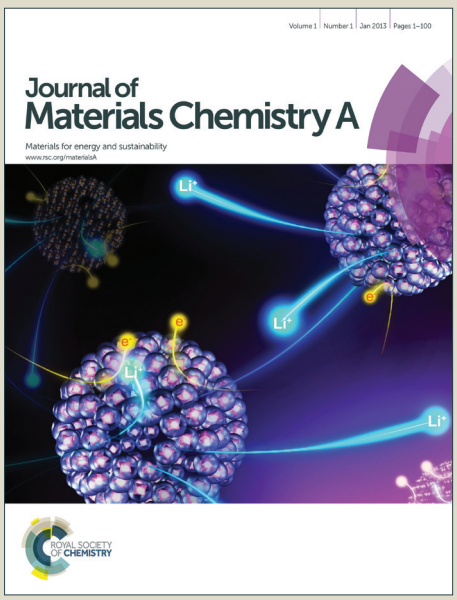

ROYAL SOCIETY OF CHEMISTRY

www.rsc.org/materialsA

Journal Of Materials Chemistry A

Cite this: DOI: 10.1039/c0xx00000x

www.rsc.org/xxxxxx

PAPER

Facile synthesis of $ZnCo_2O_4$ nanowire cluster arrays on Ni foam for High-performance Asymmetric Supercapacitors

Bingkun Guan, Di Guo, Lingling Hu, Guanhua Zhang, Tao Fu, Weiji Ren, Jidong Li and Qiuhong Li*

$ZnCo_2O_4$ nanowire cluster arrays (NWCAs) were directly grown on Ni foam via a facile hydrothermal method. The resulting products were analyzed by using X-ray diffraction spectroscopy (XRD), scanning electron microscopy (SEM), and transmission electron microscopy (TEM). The $ZnCo_2O_4$ NWCAs on Ni foam were directly used as integrated electrodes for supercapacitors and exhibited a high specific capacitance of 4.05 F cm^{-2} at 20 mA cm^{-2} (1620 F g^{-1} at 8 A g^{-1}) in 3 M KOH aqueous solution, and an excellent cycling ability at various current densities up to 100 mA cm^{-2} (40 A g^{-1}), 90% of the initial capacitance remained after 6000 cycles. Moreover, the asymmetric supercapacitor had a high energy density of 41.00 Wh kg^{-1} at a power density of 384 W kg^{-1} and 16.63 Wh kg^{-1} at a high power density of 2561 W kg^{-1}. Such excellent rate property and superior cycling life, suggest that $ZnCo_2O_4$ NWCAs can not only be applied in high energy density fields, but also used in high power density applications.

1. Introduction

In recent years, owing to increasing concern about the depletion of fossil fuels and environmental pollution, there is an urgent need for clean, efficient, and sustainable sources of energy to maintain a sustained, healthy and rapid economic development. As two of the most promising energy storage devices for electric energy storage, lithium-ion batteries (LIBs) and supercapacitors (SCs) have attracted worldwide attention. Especially, supercapacitors have attracted attention owing to their fast recharge ability, high power performance, long cycle life, and low maintenance cost,[1,2] which allow applications for various power and energy requirements, such as hybrid electric vehicles, short-term power sources for mobile electronic devices, etc.[3-5] They can complement or even replace batteries in electrical energy storage and harvesting applications, when high power delivery or uptake is needed.[1] Supercapacitors can be divided into two types, that is, store energy using either ion adsorption (electrochemical double layer capacitors) and fast surface redox reactions (pseudocapacitors). Generally, pseudocapacitors have higher energy density than the double-layer capacitors.[6,7] Therefore, most of current research has been focused on pseudocapacitors, and kinds of new capacitive materials including metal oxides, metal sulfides and conductive polymers with high energy density and long cycle life have been developed. In addition, novel materials should have as high specific surface area as possible because the storage capacitance is mainly decided by the surface redox reaction of active materials.

Cobalt, ruthenium, manganese, nickel, molybdenum, vanadium based oxides and sulfides are extremely interested in the design of high energy density pseudocapacitor electrodes[8-12] because these materials have a variety of oxidation states for charge transfer and high mass densities. As one of the most wonderful pseudocapacitive materials, ruthenium oxide (RuO_2) has exhibited excellent high specific capacitance, good electrical conductivity, and high chemical stability.[13,14] However, the high cost and rareness of Ru element limit their application in supercapacitors. Therefore, low-cost transition metal oxides, such as MnO_2,[15-17] Fe_2O_3,[18] NiO[19] and Co_3O_4[20] have been developed as candidates. Nevertheless, these binary oxides usually showed poor conductivity for supercapacitors. MnO_2 electrode exhibited excellent stability. However, the poor conductivity of MnO2 (10^{-5} - 10^{-6} S/cm) remains a major challenge and limits the rate capabilities for high power performance, thus hindering its wide applications in energy storage systems.[21] And NiO has high resistivity, which is a serious defect for supercapacitors. It is crucial to enhance the electrode conductivity in order to improve the energy density and power density of electrodes. Moreover, the specific surface area of novel materials is directly related to the specific capacitance. However, the specific surface area of the NiO is in general not high enough for high capacitance.[22] Nanostructured Co_3O_4 has been demonstrated to be a promising material of supercapacitors electrode owing to its high specific capacitance (theoretical specific capacitance up to 3560 F g^{-1}), good retention capability and high redox reactivity.[12,23,24] However, the toxicity and high cost of Co, researches have to consider to make inexpensive and environment friendly alternative metals partially instead of Co_3O_4. Due to the transition metal oxides have a serious defect for supercapacitors. Therefore, most current research has been focused on ternary oxide materials and a series of ternary oxides have been developed, $CoMoO_4$,[25] $ZnWO_4$,[26] Zn_2SnO_4.[27] They exhibit higher performance due to the synergy effects: one metal oxide displays feasible oxidation state and shows high capacity, and one shows high conductivity. Therefore, they can greatly enhance both the capacitance and durability of electrodes. And the family of cobalt-based metal oxides such as $NiCo_2O_4$,[28,29] $MnCo_2O_4$,[30] and $ZnCo_2O_4$,[31,32] are isostructural to Co_3O_4. They can not only improve the electrochemical performance over single component oxides but also offer other advantages including low cost, abundant resources and environmental friendliness. $ZnCo_2O_4$ is typical for this consideration. Zn ions occupy the tetrahedral sites in the cubic spinel structure, and the trivalent Co ions occupy the octahedral sites. Zinc compounds with good electrical

conductivity can improve its electrical conductivity and capacitive performance.[33,34] Therefore, $ZnCo_2O_4$ can be considered as a promising electrode for supercapacitors.

In this work, $ZnCo_2O_4$ nanowire cluster arrays (NWCAs) directly grown on Ni foam were developed by a simple hydrothermal route together with a annealing treatment in pure argon at 400 °C for 2 h, and the application in supercapacitors was systematically studied. The $ZnCo_2O_4$ NWCAs manifested apparent advantages as follows: firstly, $ZnCo_2O_4$ NWCAs as one-dimensional (1D) array architecture showed obvious advantages, such as high aspect ratio, high interfacial area and fast electrical pathways, compared with other nanostructure materials.[35-37] Secondly, the NWCAs directly grow on Ni foam could provide numerous express pathways for fast electron-transport without any need to incorporate binders and carbon black to overcome additional undesirable interfaces and defects, resulting in reduced internal resistance to enhance the rate capability.[25,26,38] Thirdly, the excellent structural stability of the NWCAs electrodes could improve the cycling stability and high rate capability evidently during long-term cycling at high current densities. [25] Based on the above advantages, the as-prepared Ni foam supported $ZnCo_2O_4$ NWCAs for supercapacitors exhibited a high specific capacitance 4.05 F cm^{-2} (1620 F g^{-1}) at a current density of 20 mA cm^{-2} (8 A g^{-1}), even 2.95 F cm^{-2} (1180 F g^{-1}) at a higher current density of 50 mA cm^{-2} (20 A g^{-1}). Moreover, the electrode displayed excellent cycling ability (40 A g^{-1}), and 90% of the initial capacitance remained after 6000 cycles at 20 mA cm^{-2}. Finally, we fabricated asymmetric supercapacitor with $ZnCo_2O_4$ NWCAs and active carbon as two electrodes. It exhibited high energy densities of 41.00 and 16.63 Wh kg^{-1} at power densities of 384 and 2561 W kg^{-1}, respectively, which showed the $ZnCo_2O_4$ NWCAs were a promising material for supercapacitors.

2. Experimental details

Chemical materials

In the experiment, all chemicals were of analytical grade and used without any purification process, including Ni foam substrate (specific surface area, 0.00286 m^2 g^{-1}; porosity ≥ 95 %), zinc nitrate hexahydrate ($Zn(NO_3)_2 \cdot 6H_2O$, Tianjin Chemicals, 99.5%), cobalt nitrate hexahydrate ($Co(NO_3)_2 \cdot 6H_2O$, Tianjin Chemicals, 99.0%), ammonium fluoride (NH_4F, Tianjin Chemicals, 96.0%), urea ($CO(NH_2)_2$, Tianjin Chemicals, 99.0%), and the deionized water was Millipore Milli-Q grade with a resistivity larger than 18 MΩ cm^{-1}.

Fabrication of $ZnCo_2O_4$ NWCAs on Ni foam

Ni foam supported-$ZnCo_2O_4$ NWCAs was prepared via a template-free growth method. In a typical experiment, after degreased with acetone, the Ni foam substrate (8×4×0.1 cm) was cleaned and etched with 6 M HCl in an ultrasound for 20 min to remove the surface NiO layer, and then rinsed with deionized water and absolute ethanol for 30 min respectively. Then the Ni foam was placed standing against the wall of Teflon-lined autoclave (130 mL).

For the hydrothermal method, $Zn(NO_3)_2 \cdot 6H_2O$ (0.595 g) and $Co(NO_3)_2 \cdot 6H_2O$ (1.164 g) were dissolved separately in 30 mL of deionized water with magnetic stirring. At the same time, NH_4F (0.148g, 4 mmol) and $Co(NH_2)_2$ (0.601 g) were dissolved in the mixture of 20 mL deionized water and 20 mL ethanol with magnetic stirring. After stirring for 30 min, the zinc nitrate solution was added slowly to the cobalt nitrate solution. Then, the mixture of ammonium fluoride and urea was added to the mixture of zinc nitrate and cobalt nitrate, again with magnetic stirring for 30 min at room temperature. Then the resulting solution was transferred into the above Teflon-lined autoclave. Subsequently, the autoclave was sealed and put into an electronic oven and maintained at 120°C for 16 h. When the hydrothermal reaction was finished, the autoclave was cooled to ambient temperature naturally, and the Ni foam coated with a pink product was taken out from the autoclave and washed carefully by distilled water and absolute alcohol in an ultrasound for several times in order to remove the residual nanoparticle, then dried in an oven at 60 °C for 8 h. Finally, the samples were annealed at 400 °C for 2 h in pure argon with a heating rate of 2 °C min^{-1} to obtain $ZnCo_2O_4$ NWCAs.

Characterization

The crystal structure of the $ZnCo_2O_4$ NWCAs was observed by X-ray powder diffraction (XRD, Cu Kα irradiation; λ=1.5408 Å) with a SIEMENS D5000 X-ray diffractometer. The morphology and microstructure of the synthesized sample were examined by a scanning electron microscopy (SEM, Hitachi S4800 equipped with an EDS) and a transmission electron microscope (TEM, JEOL-2010 with an accelerating voltage of 200 kV).

Electrochemical Measurements

All electrochemical measurements were carried out in a three electrode electrochemical cell containing 3 M KOH aqueous solution as the electrolyte at room temperature. The $ZnCo_2O_4$ NWCAs on Ni foam (1× 1 cm^2) acted as the working electrode, and a saturated calomel electrode (SCE) and a platinum plate were used as a reference and counter electrode, respectively. The mass loading of the active material on Ni foam was about 2.5 mg cm^{-2}. The area specific capacitance (ASC) of the electrode is calculated according to the following equations: [11,12]

$$C = \frac{\int i \times d\Delta u}{v \times \Delta u \times s} \qquad (1)$$

$$C = \frac{i \times t}{\Delta u \times s} \qquad (2)$$

Where Δu is the potential (V), v is the potential scan rate (mV s^{-1}), i is the discharging current (A), t is discharge time (s), and s is the geometrical area of the electrode (cm^2). The cyclic voltammetry (CV) measurements and galvanostatic charge-discharge tests were performed on a CHI660e electrochemical workstation (Chenhua, Shanghai). Electrochemical impedance spectroscopy (EIS) tests were performed by a superimposed 5 mV sinusoidal voltage in the frequency range of 100 kHz-0.01 Hz at open circuit potential.

Asymmetric supercapacitor devices

An asymmetric supercapacitor was made by using activated carbon film on Ni foam(1× 1 cm^2) as the negative electrode and $ZnCo_2O_4$ NWCAs on Ni foam(1× 1 cm^2) as the positive electrode with one piece of cellulose paper as the separator in 3 M KOH as the electrolyte. According to a series of comparative experiments, 7.8 mg of activated carbon was chosen to balance the capacitance of the two electrodes. So the total mass of the two active electrode materials is 10.3 mg cm^{-2}.

3. Results and discussion

The hydrothermal synthesis procedure is illustrated in Fig. 1. A simple hydrothermal method together with a post annealing process resulted in a high density of $ZnCo_2O_4$ NWCAs standing vertically on Ni foam. Fig. 1(a) showed the morphological evolutions of the products obtained at different reaction stages (0, 0.5, 6 and 16 h) while keeping the other experimental conditions such as the reactants concentration and temperature unchanged. From the SEM images (Fig. 1(a)), the growth process was proposed as shown in Fig. 1(b). Before reaction, the surface of Ni foam substrate was smooth, in the first 0.5 h of the hydrothermal process, numerous $ZnCo_2O_4$ precursor ($Zn_xCo_{2x}(OH)_{6x}$) nanoseeds derived from combination of the Zn^{2+}, Co^{2+} and OH^- ions.[39,40] And it was a nucleation stage, and many nanoparticles could be seen at the end of this stage. With the reaction proceeding, the crystal growth stage transferred to a kinetically controlled process, and small nanowires began to grow from the nucleation site.[25] At the end of 6h, the Ni foam surface was covered with nanowires. The nanowires continued to grow, and formed nanowire clusters at the end of 16 h.

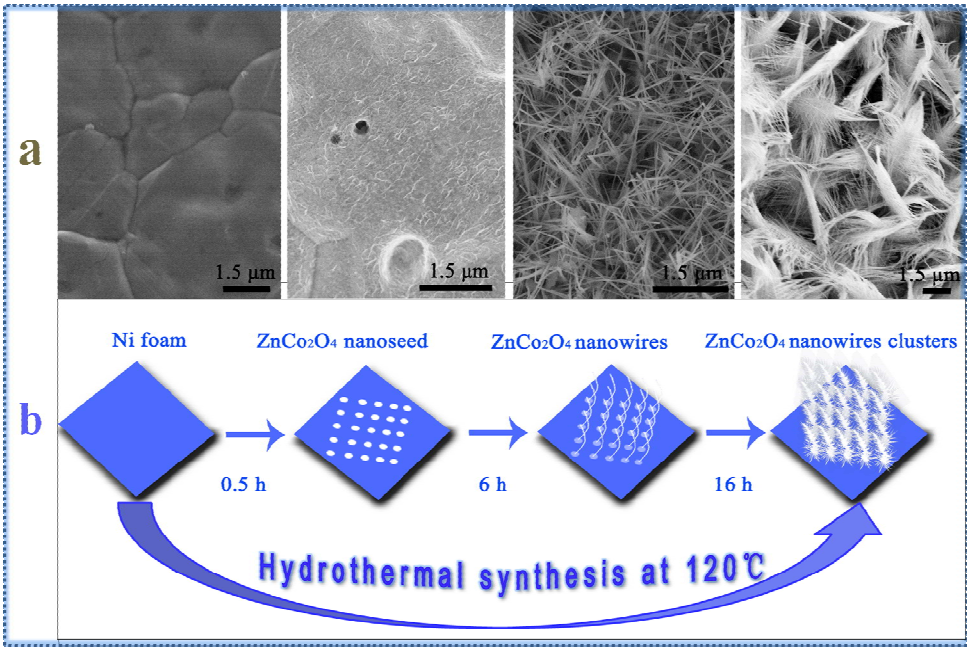

Fig. 1 (a) SEM images and (b) schematic illustration of the growth processes of $ZnCo_2O_4$ NWCAs on Ni foam

Figure 2 shows low and high magnification images of the final products after annealing. The morphology did not change obviously after annealing.

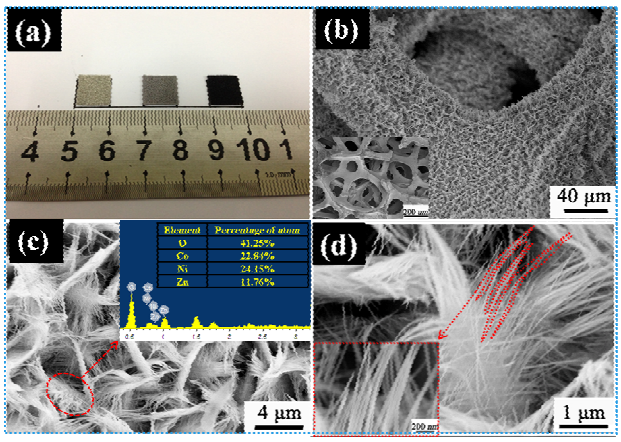

Fig. 2 (a) Photographs of Ni foam substrate (left), precursors grown on Ni foam (middle) and the sample after annealing (right); (b, c) top-view SEM images of $ZnCo_2O_4$ NWCAs on Ni foam, inset in Figure 2 (b) is the nickel foam after $ZnCo_2O_4$ NWCAs growth and inset in Figure 2 (c) is the EDS result of the hybrid clusters; (d) SEM image of $ZnCo_2O_4$ NWCAs, inset: the high magnification image of the nanowires. The diameter of the nanowire is about 20 to 40 nm.

From Fig. 2(a), the bare Ni foam (left) was lightly gray. It turned to pink after the hydrothermal process (middle), and then to black (right) after annealing treatment at 400 °C for 2 h under Ar flow. More importantly, $ZnCo_2O_4$ NWCs stood on nickel foam while still keeping excellent flexibility of the bare nickel foam, which was helpful for flexible energy storage applications. Fig. 2(b) and its inset showed the SEM images of final Ni foam with $ZnCo_2O_4$ NWCAs, indicating that the NWCAs with high density covered the entire Ni skeletons.

The EDS spectrum as shown in the inset of Fig. 2(c) indicated that presence of Zn, Co, O and Ni arose from the Ni foam substrate. As shown in Fig. 2(d), the vertically aligned feather-like nanowires on Ni foam substrate could provide large active surface area, much shorter paths for electron transport and effective channels for the electrolyte.

The composition and phase structure of the products were analyzed by XRD, and the results revealed that $ZnCo_2O_4$ was obtained after an annealing process. In order to eliminate the strong impact of Ni foam substrate on the XRD diffraction peaks

signals, the product powder was scratched from Ni foam. As can be seen from Fig. 3(a), all the diffraction peaks can be indexed to (111), (220), (311), (222), (422), (511), (440) and (533) planes of the cubic $ZnCo_2O_4$ phase, consistent with the standard card (JCPDF card no. 23-1319). A small amount of $ZnCo_2O_4$ nanowires were removed from the Ni foam substrate after a strong ultrasonic treatment for 30 minutes in ethanol, and then collected for TEM analysis. The crystal structure and morphologies of the $ZnCo_2O_4$ nanowires were further characterized in Fig. 3(b, c, d). As seen from Fig. 3(b), the diameter distribution of $ZnCo_2O_4$ nanowire was at about 20 nm, which matched well with the SEM results above. Fig. 3(b) and (c) showed that these $ZnCo_2O_4$ nanowires were actually assembled by very small nanocrystals with the size ranging from 10 to 15 nm. The nanocrystals interconnected with each other and formed a stable nanowire with very small pores. Obviously, these pores could greatly improve the surface-to-volume ratio of the nanowires. The unique mesoporous characteristic of $ZnCo_2O_4$ is advantageous for electrolyte diffusion and fast electron transport which may facilitate the electrochemical activity.

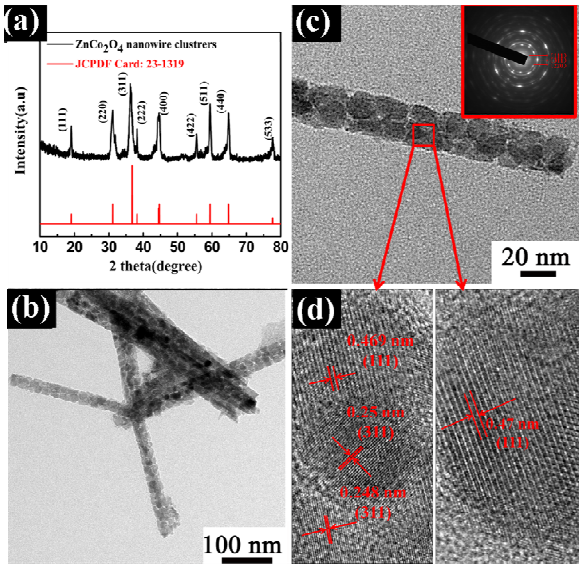

Fig. 3 (a) The typical XRD pattern of the annealed $ZnCo_2O_4$ nanowires scratched from Ni foam. TEM micrographs of the synthesized nanostructures, (b, c) TEM images of the $ZnCo_2O_4$ and inset in (c) shows a corresponding SAED pattern on an individual nanowire; (d) High-resolution TEM images of the $ZnCo_2O_4$ nanowire.

The corresponding selected-area electron diffraction (SAED) pattern is shown in the inset of Fig. 3(c), which exhibited periodic diffraction spots, demonstrating the nano-crystalline nature of the compound. The calculated *d* values of 0.47, 0.28, and 0.25 nm corresponded to the (111), (220) and (311) Miller indices, respectively, in accordance with the XRD results of $ZnCo_2O_4$ (Fig. 3(a)). High-resolution TEM (HRTEM) image (Fig. 3(d)) was taken from the parts of the region highlighted by a red rectangle in Fig. 3(c). The lattice fringes showed the structural characteristic of cubic spinel $ZnCo_2O_4$ crystal, in which the interplanar spacing about 0.25 nm and 0.47 nm corresponded to the (311) and (111) planes, respectively.

Cyclic voltammetry (CV) and chronopotentiometry (CP) tests were conducted in a three-electrode system with 3 M KOH aqueous solution as the electrolyte. Cyclic voltammetry (CV) of self-supported $ZnCo_2O_4$ NWCAs on Ni foam within the potential range of 0.05 to 0.65 V at various scan rates (5, 10, 30, 50 mV s^{-1}) were shown in Fig. 4(a). The CV curves consisted of a pair of strong redox peaks, which indicated that the capacitance characteristics were mainly governed by Faradaic redox reactions. At a low scan rate of 5 mV s^{-1}, the anodic peak at 0.53 V was due to the oxidation process, while the cathodic peak at about 0.32 V was related to its reverse process. The pair of peaks was assigned to the $Co(OH)_2$/CoOOH redox couple prior to the onset of oxygen evolution.[30-42] The redox reactions in the alkaline electrolyte are based on the following equations:

$$Co_2O_4^{2-} + 2H_2O \leftrightarrow 2CoOOH + 2OH^- \quad (3)$$

$$CoOOH + H_2O + e^- \leftrightarrow Co(OH)_2 + OH^- \quad (4)$$

The anodic and cathodic peaks shifted to more anodic and cathodic directions with the increase of the scan rate from 5 to 50 mV s^{-1}, respectively, which indicated the kinetic irreversibility in the redox process due to polarization and ohmic resistance during the Faradaic process in $ZnCo_2O_4$ NWCAs.[43-45]

Fig. 4(b) shows the galvanostatic charge-discharge results at different current densities (20, 30, 50, 80 and 100 mA cm^{-2}) with the voltage between 0 and 0.6 V. The discharge curves in Fig. 4(b) showed a significant deviation from a straight and flat line, indicating that the capacitance was mainly caused by the Faradaic redox reactions, so the existence of plateaus in the discharge curves suggested typical pseudocapacitive characteristics, which is consistent with the CV curves (Fig. 4(a)). The ASC of $ZnCo_2O_4$ NWCAs electrode was calculated from discharge time according to the equation (2), which was about 4.05, 3.48, 2.95, 2.12 and 1.67 F cm^{-2} at current densities of 20, 30, 50, 80 and 100 mA cm^{-2}, respectively. As shown in. Fig. 4(c), with the increase of discharge current density, ASC gradually decreased because of the incremental potential drop and relatively insufficient active material involved in redox reaction under higher current densities At a high current density of 100 mA cm^{-2} (40 A g^{-1}), the electrode still revealed a high capacitance of 1.67 F cm^{-2} (668 F g^{-1}), demonstrating good rate capability.

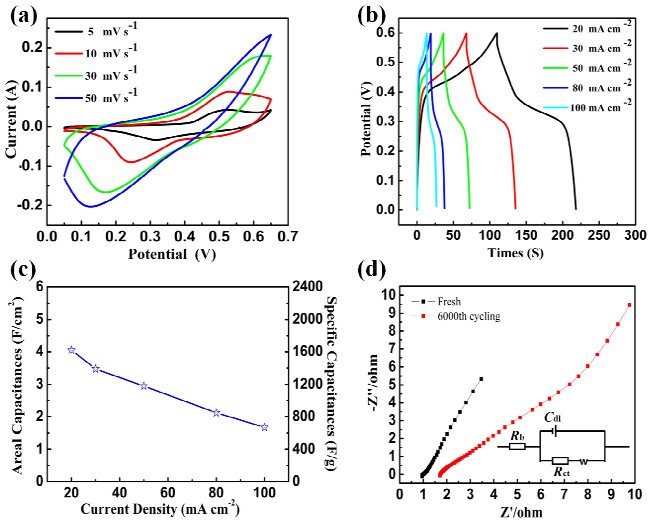

Fig. 4 (a) CV curves of $ZnCo_2O_4$ NWCAs at various scan rates; (b) galvanostatic charge/discharge curves of the $ZnCo_2O_4$ electrode at different current densities; (c) ASC of $ZnCo_2O_4$ NWCAs (2.5 mg cm^{-2}) at

various discharge current densities; (d) Nyquist curve of the $ZnCo_2O_4$ NWCAs before and after 6000 cycling at open circuit potential.

Electrochemical impedance spectroscopy (EIS) was measured and the corresponding Nyquist plots were shown in Fig. 4(d). In the high frequency area, the intersection of the curve at real part Z', which is equal to internal resistances (R_b), indicates the bulk resistance of the electrochemical system. R_b for the $ZnCo_2O_4$ NWCAs electrode increased from 0.9 Ω to 1.7 Ω after 6000 cycles, indicating a slight electron conductivity decrease of the electrode. The low charge-transfer resistance (R_{ct}) represented by the high-frequency semicircle indicates the large electroactive surface area of the electrode. The diffusive resistance (Warburg impedance) of $ZnCo_2O_4$ NWCAs electrode represented by the slope in low-frequency curve was a little higher after 6000 cycles. These results could be related to a slight change in surface and microstructure of the $ZnCo_2O_4$ NWCAs after 6000 successive cycles.

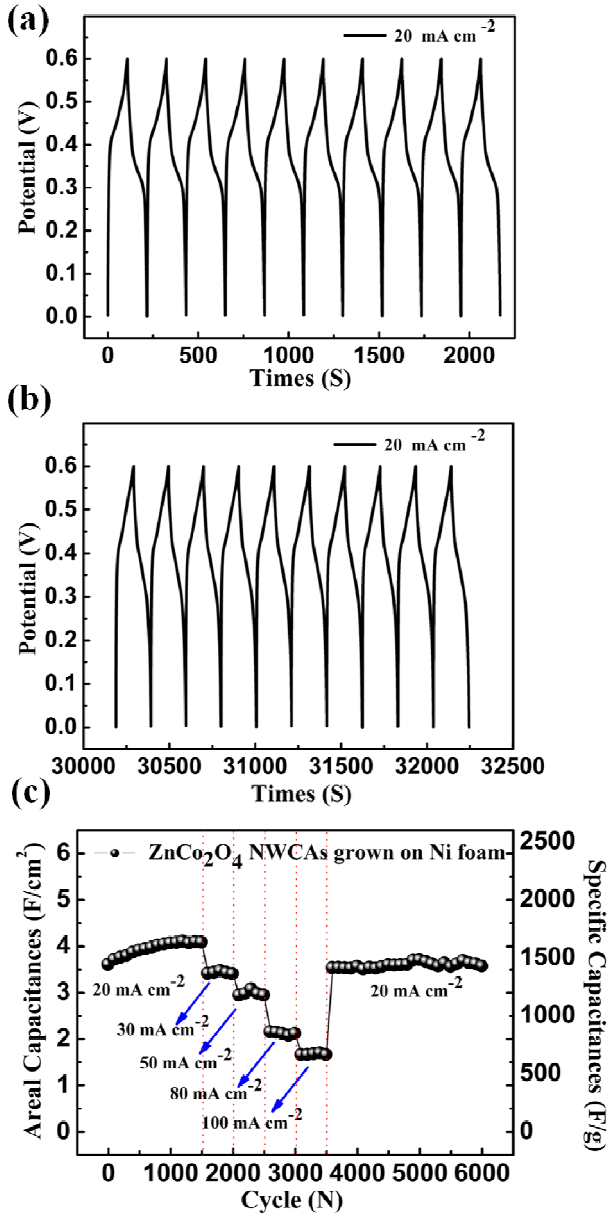

Fig. 5 (a) The first and (b) last ten galvanostatic charge and discharge voltage profiles at 20 mA cm^{-2}; (c) cycling performance of Ni foam supported $ZnCo_2O_4$ NWCAs electrodes under various current densities for 6000 cycles.

Long cycle stability is another critical requirement for practical applications of supercapacitors. The cycle stability of $ZnCo_2O_4$ NWCAs electrodes was tested by repeated charge-discharge processes in the range of 0-0.6 V in 3 M KOH aqueous solution. Fig. 5(a) and (b) showed that first and last ten cycles of representative voltage profiles at a current density of 20 mA cm^{-2}. The ASC reduced about 10% after 6000 cycles, suggesting that the $ZnCo_2O_4$ NWCAs electrode had excellent cycling stability and good reversible redox behaviors. From Fig. 5(c), during the first 1500 cycles at 20 mA cm^{-2} (8 A g^{-1}), the ASC was increasing, and finally maintained at about 4.05 F cm^{-2} (1620 F g^{-1}). The capacitance increase (12 %) was observed mainly during the first 600 cycles, which is attributed to the activation process of the active materials in the electrolyte. With the cycle number increasing, the electrolyte diffused to the inter $ZnCo_2O_4$ absolutely and opened up the ion access. After continuously cycling at 30, 50, 80 and 100 mA cm^{-2} for respective 500 times, the current densities turned back to 20 mA cm^{-2}, and 90% of the initial capacitance (3.66 F cm^{-2}) was still remained and maintained for the last 3000 cycles without noticeable decrease. Furthermore, the specific capacitance reported here was much higher than those reported $ZnCo_2O_4$ in table 1, such as $ZnCo_2O_4$ nanotubes (596.2 F g^{-1} at 20 A g^{-1}),[46] and the $ZnCo_2O_4$ Nanorods/Ni foam (1015 F g^{-1} at 20 A g^{-1}).[40]

Electrode materials	Current density	Specific capacitance	Reference
$ZnCo_2O_4$ NWCAs	50 mA cm^{-2} (20 A g^{-1})	2.95 F cm^{-2} (1180 F g^{-1})	This our work
$ZnCo_2O_4$ nanotubes	20 A g^{-1}	596.2 F g^{-1}	Ref. 46
$ZnCo_2O_4$ Nanorods	20 A g^{-1}	1015 F g^{-1}	Ref. 40

Table.1. Summarization of the supercapacitor performance of different $ZnCo_2O_4$.

The good electrochemical property of $ZnCo_2O_4$ NWCAs electrode could be attributed to the following factors. Firstly, the Ni foam with zigzag flow channels and micro holes provided plentiful fast electron-transport accesses to the current collector. Secondly, each $ZnCo_2O_4$ nanowire with numerous mesopores can greatly increased the surface to volume ratio of nanowires. So, the structure could not only provided an effective channel for the electrolyte, but also facilitate fast intercalation and de-intercalation of active species. Thirdly, because nanowires are directly grown on Ni foam avoiding the use of carbon black and binder, all $ZnCo_2O_4$ nanowires might participate in the redox reactions, improving the utilization of active materials. Finally, the cluster structure of the nanowire was also helpful to relieve

the structure deformation which was caused by volume change during the cycling process and thus the excellent cycling stability.

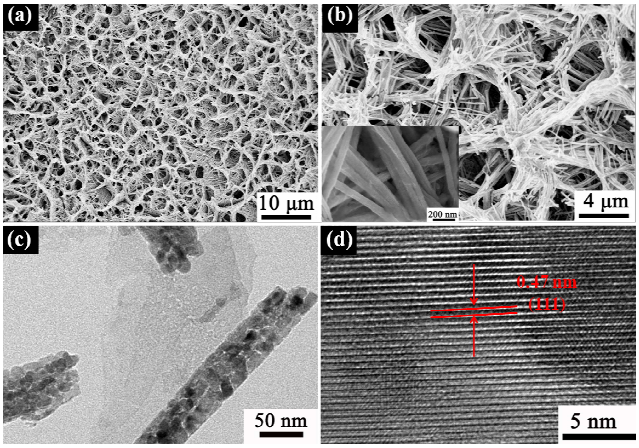

Fig. 6 (a, b) SEM images of the $ZnCo_2O_4$ NWCAs on Ni foam electrode after 6000 cycles; (c, d) TEM and HRTEM of the $ZnCo_2O_4$ NWCAs after 6000 cycles

The morphology of the $ZnCo_2O_4$ NWCAs electrode was analyzed after 6000 cycles by SEM as shown in Fig. 6(a) and (b). The basic nanowire cluster structure was barely changed as shown in Fig. 6(a) and still strongly adhered on the Ni foam substrate, while the nanowire became much thicker as shown in the inset of Fig. 6(b). TEM and HRTEM of the $ZnCo_2O_4$ NWCAs after 6000 cycles were also analyzed. The morphology and crystalline characteristics had not changed obviously after 6000 cycling (Fig. 6(c) and (d)), and this revealed that the structure was stable during repeated charge-discharge processes.

Finally, to investigate the $ZnCo_2O_4$ NWCAs for practical application, an asymmetric supercapacitor was made. Fig. 7a showed schematic structure of the asymmetric supercapacitor and Fig. 7b exhibited the optical image of assembled device, where the asymmetric supercapacitor was wrapped in a plastic bag. Fig. 7c revealed that a red light-emitting diode (LED) was lightened by two asymmetric supercapacitor devices in series. In the devices, the supercapacitors and the red LED was connected in platinum wire (0.5mm). Then, the asymmetric supercapacitors were charged to 3.2 V and a 5 mm-diameter red round LED indicator was lighted. Fig. 7d showed the lighted LED at different stages. The LED could be powered continuously about 2 min.

The electrochemical properties of an asymmetric supercapacitor cell were measured and shown in Figs. 7(e-h). The cell voltage is 1.6 V, as shown in Fig. 7f, charge/discharge curves of the asymmetric supercapacitor at different current densities from 5 mA cm^{-2} (0.48 A g^{-1}) to 30 mA cm^{-2} (2.91 A g^{-1}) were tested. On the basis of these data, the relation between energy density and power density (E and P) was shown in Fig. 7g. The E and P were calculated according to the following equations:

$$E = \frac{\int I \times V(t) dt}{M} \quad (5)$$

$$P = \frac{E}{\Delta t} \quad (6)$$

Where I is the discharging current, $V(t)$ the discharging voltage excluding the IR drop, dt the time differential, M the total mass of the two active electrode materials, and Δt the discharging time. The energy density of our asymmetric supercapacitor device decreased from 41.00 to 16.63 Wh kg^{-1}, while the power density increased from 384 to 2561 W kg^{-1}.

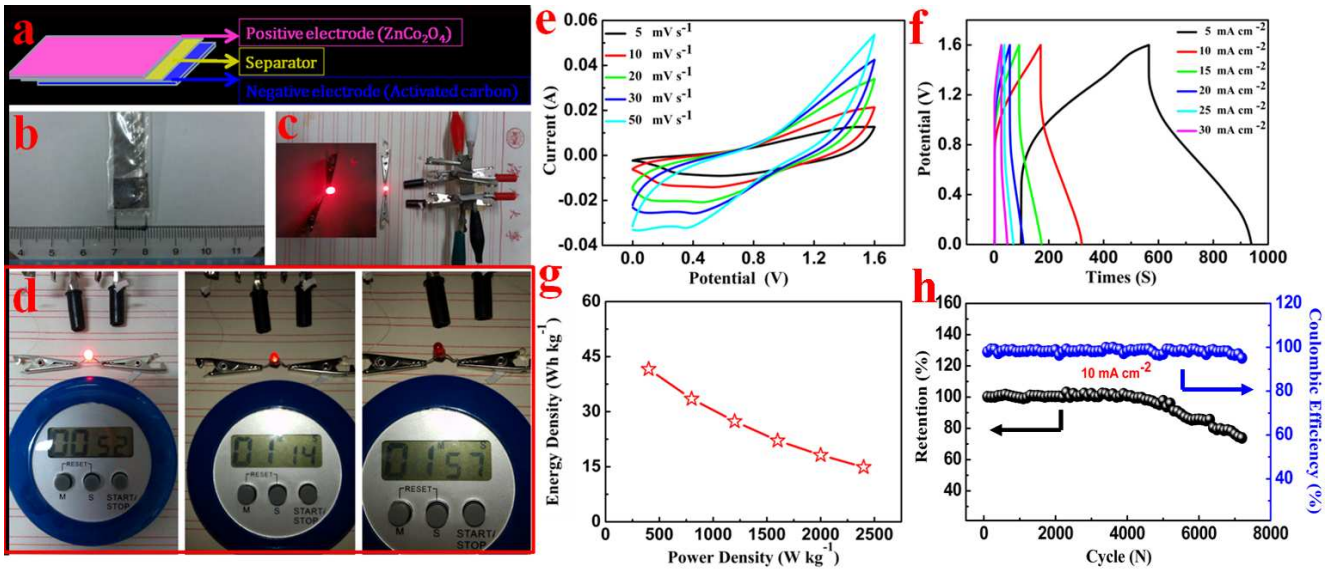

Fig. 7 (a) Schematic illustration of the asymmetric supercapacitor configuration; (b) a photograph of our asymmetric supercapacitor (c) a photograph showing that two supercapacitors in series can lighten up a red LED indicator; (d) images of the red LED at different stages. (e) CV curves of our device at various scan rates; (f) charge/discharge curves at different current densities and (g) Ragone plot of the device; (h) cycling performance of our device.

Notably, the device still had an energy density of 16.63 Wh kg^{-1} at a high power density of 2561 W kg^{-1}. We also compared the energy density/power density of our work with those previously reported works, such as $NiCo_2O_4$@MnO_2 coreshell nanowire

arrays on Ni foam (energy density 35 Wh kg^{-1} at a power density of 163 W kg^{-1}),[47] Co_3O_4@MnO_2 coreeshell arrays on Ni foam (energy density 17.7 W h kg^{-1} at a power density of 600 W kg^{-1}),[48] Ni-Co sulfide nanowires on Ni foam (25Wh kg^{-1} at a high power density of 447 kW kg^{-1}),[49] and etc. And the energy density in our work is higher than those symmetrical supercapacitors, such as CNTs//CNTs supercapacitors (<10 W h kg^{-1}),[50] AC//AC supercapacitors (<10Wh kg^{-1}),[51] rGO//rGO supercapacitors (<4 W h kg^{-1}).[52]

The cycling performance of the device up to 7000 times at a current density of 10 mA cm^{-2} (0.97 A g^{-1}) was shown in Figure 7h, the cycle retention was remained about 78 % of the initial capacity, and the Clombic efficiency was above 98.4 % in the cycles, which indicated that the Faraday reactions behaved irreversibility or induced a degradation of the microstructure during the cycle test.

4. Conclusion

In summary, the $ZnCo_2O_4$ NWCAs on Ni foam were synthesized for high-performance supercapacitors by a simple hydrothermal method together with a post annealing treatment in pure argon. The $ZnCo_2O_4$ NWCAs electrodes showed high electrochemical performance with a high specific capacitance of 4.05 F cm^{-2} (1620 F g^{-1}) at a current density of 20 mA cm^{-2} (8 A g^{-1}), even 2.95 F cm^{-2} (1180 F g^{-1}) at a higher current density of 50 mA cm^{-2} (20 A g^{-1}). Moreover, 90% of the initial capacitance was maintained after more than 6000 charge/discharge cycles at different current densities from 20 to 100 mA cm^{-2}. In addition, the asymmetric supercapacitor had a high energy densityof 41.00 Wh kg^{-1} at a power density of 384 W kg^{-1} and 16.63 Wh kg^{-1} at a high power density of 2561 W kg^{-1}. Such high specific capacitance, excellent rate capability and cycling stability for high-performance supercapacitors could be mainly ascribed to the unique porous $ZnCo_2O_4$ NWCAs structure directly growing on Ni foam, which could provide high aspect ratio, high interfacial area and fast electron and ion pathways and therefore enhance the electrochemical reaction. The strategy will promote the development for high performance supercapacitor electrodes.

Acknowledgements

This work was partly supported by the National Natural Science Foundation of China (Grant No.61376073), the Specialized Research Fund for the Doctoral Program of Higher Education of China (20120161110016), the Hunan Provincial Natural Science Foundation of China (Grant No. 11JJ7004), and the Hunan Provincial Major Project of Science and Technology Department (Grant No. 2012TT1004).

Notes and references

Key Laboratory for Micro-Nano Optoelectronic Devices of Ministry of Education, and State Key Laboratory for Chemo/Biosensing and Chemometrics, Hunan University, Changsha, 410082, P. R. China. E-mail:liqiuhong2004@hotmail.com. Tel.: +86 0731 88664019; Fax: +86 0731 88822137.

1 P. Simon and Y. Gogotsi, *Nat. Mater*, 2008, **7**, 845.
2 J. R. Miller and P. Simon, *Science*, 2008, **321**, 651.
3 B. E. Conway, *J. Electrochem. Soc*, 1991, **138**, 1539.
4 T. Stimpfling and F. Leroux, *Chem. Mater*, 2010, **22**, 974.
5 B. Andrew, *J. Power Source*, 2000, **91**, 37.
6 C. Z. Yuan, B. Gao, L. F. Shen, S. D. Yang, L. Hao, X. J. Lu, F. Zhang, L. J. Zhang and X. G. Zhang, *Nanoscale*, 2011, **3**,529.
7 J. P. Liu, J. Jiang, M. Bosman and H. J. Fan, *J. Mater. Chem*, 2012, **22**, 2419.
8 X. Xia, J. Tu, Y. Zhang, X. Wang, C. Gu, X. B. Zhao and H. J. Fan, *ACS Nano*, 2012, **6**, 5531.
9 L. L. Zhang, R. Zhou and X. S. Zhao, *J. Mater. Chem*, 2010, **20**, 5983.
10 T. Brezesinski, J. Wang, S. H. Tolbert and B. Dunn, *Nat Mater*, 2010, **9**, 146-151.
11 G. H. Zhang, T. H. Wang, X. Z. Yu, H. N. Zhang, H. G. Duan and B. A. Lu, *Nano energy*, 2013, **2**, 586.
12 H. N. Zhang, Y. J. Chen, W. W. Wang, G. H. Zhang, M. Zhuo, H. M. Zhang, T. Yang, Q. H. Li and T. H. Wang, *J. Mater. Chem. A,* 2013, **1**, 8593.
13 J. P. Zheng and T. R. Jow, *J. Electrochem. Soc,* 1995, **142**, 6.
14 J. P. Zheng, P. J. Cygan, T.R. Jow, *J. Electrochem. Soc*, 1995, **142**, 2699.
15 X. H. Lu, D. Z. Zheng, T. Zhai, Z. Q. Liu, Y. Y. Huang, S. L. Xie and Y. X. Tong, *Energy Environ. Sci*, 2011, **4**, 2915.
16 A. J. Roberts and R. C. T. Slade, *J. Mater. Chem*, 2010, **20**, 3221.
17 Y. Zhang, G. Y Li, Y. Lv, L. Z. Wang, A. Q. Zhang, Y. H. Song and B. L. Huang, *Int. J. Hydrogen Energy*, 2011, **36**, 11760.
18 X. H. Xia, J. P. Tu, Y. J. Mai, X. L. Wang, C. D. Gu and X. B. Zhao, *J. Mater. Chem,* 2011, **21**, 9319.
19 J. W. Lee, T. Ahn, J. H. Kim, J. M. Ko and M. D. Kim, *Electrochim. Acta*, 2011, **56**, 4849.
20 K. Xie, J. Li, Y. Q. Lai, W. Lu, Z. Zhang, Y. X. Liu, L. Zhou and H. T. Huang, *Electrochem. Commun*, 2011, **13**, 657.
21 D. Belanger, T. Brousse, J. W. Long, *Electrochem. Soc. Interfaces*, 2008, **17**, 49.
22 J. Y. Lee, K. Liang, K. H. Ana and Y. H. Lee, *Synthetic Metals* 2005,**150**, 153.
23 J. P. Liu, J. Jiang, C. W. Cheng, H. X. Li, J. X. Zhang, H. Gong and H. J. Fan, *Adv. Mater*, 2011, **23**, 2076.
24 X. H. Xia, J. P. Tu, X. L. Wang, C. D. Gu and X. B. Zhao, *Chem. Commun,* 2011, **47**, 5786.
25 D. Guo, H. M. Zhang, X. Z. Yu, M. Zhang, P. Zhang, Q. H. Li and T. H. Wang, *J. Mater. Chem. A*, 2013, **1**, 7247.
26 B. K. Guan, L. L. Hu, G. H. Zhang, D. Guo, T. Fu, J. D. Li, H. G. Duan and Q. H. Li, *RSC Adv,* 2014, **4**, 4212.
27 H. W. Wang, Z. A. Hu, Y. Q. Chang, Y. L. Chen, H. Y. Wu, Z. Y. Zhang and Y. Y. Yang, *J. Mater. Chem*, 2011, **21**, 10504.
28 L. H. Bao, J. F. Zang, and X. D. Li, *Nano Lett.*, 2011, **11**, 1215.
29 L. Yu, G. Q. Zhang, C. Z. Yuan and X. W. Lou, *Chem. Commun*, 2013, **49**, 137.
30 J. Gomez and E. E. Kalu, *J. Power Sources*, 2013, **230**, 218.
31 K. Karthikeyan, D. Kalpana and N. G. Renganathan, *Ionics*, 2009, **15**, 107.
32 L. L. Hu, B. H. Qu, C. C. Li, Y. J. Chen, L. M, D. N. Lei, L. B. Chen, Q. H. Li and T. H. Wang, *J. Mater. Chem. A*, 2013, **1**, 5596.
33 Y. B. He, G. R. Li, Z. L. Wang, C. Y. Su, Y. X. Tong, *Energy Environ. Sci*, 2011, **4**, 1288.
34 L. H. Bao, J. F. Zang, X. D. Li, *Nano Lett*, 2011, **11**, 1215.
35 Y. Y. Gao, S. L. Chen, D. X. Cao, G. L. Wang and J. L Yin, *J. Power Sources*, 2010, **195**, 1757.
36 G. X .Wang, X. P. Shen, J. Horvat, B. Wang, H. Liu, D. Wexler, J. Yao, *J. Phys. Chem. C*, 2009, **113**, 4357.
37 H. Zhang, J. B. Wu, C. X. Zhai, X. Y. Ma, N. Du, J. P. Tu and D. R. Yang, *Nanotechnology*, 2008, **19**, 035711.
38 D. N. Lei, M. Zhang, B. H. Qu, L. B. Chen, Y. G. Wang, E. D. Zhang, Z. Xu, Q.H. Li and T. H. Wang, *Nanoscale*, 2012, **4**, 3422.
39 C. Z. Yuan, J. Y. Li, L. R. Hou, X. G. Zhang, L. F. Shen and X. W. Lou, *Adv Funct Mater*, 2012, **22**, 4592.
40 B. Liu, B. Y. Liu, Q. F. Wang, X. F. Wang, Q. Y. Xiang, D. Chen and G. Z. Shen. *Appl. Mater. Interfaces*, 2013, **10**, 1021
41 H. L. Wang, Q. M. Gao and L. Jiang, *Small*, 2011, **7**, 2454.
42 L. L. Li, S. J. Peng, Y. L. Cheah, P. F. Teh, J. Wang, G. Wee, Y. W. Ko, C. L. Wong and M. H. Srinivasan, *Chem. Eur. J*, 2013, **19**, 5892.
43 P. Justin, S. K. Meher and G. R. Ranga, *J. Phys. Chem,* 2010, **114**, 5203.

44 W. G. Pell and B. E. Conway, *J. Electroanal. Chem*, 2001, **500**, 121.

45 Sumanta Kumar Meher and G. Ranga Rao. *J. Phys. Chem. C,* 2011, **115**, 15646.

46 G. Zhou, J. Zhu, Y. J. Chen, L. Mei, X. C. Duan, G. H. Zhang, L. B. Chen, B. A. Lu and T. H. Wang, *Electrochim. Acta,* DOI: 10.1016/j.electacta.2014.01.018.

47 K. B. Xu, W. Y. Li, Q. Liu, B. Li, X. J. Liu, L. An, Z. G. Chen, R. J. Zou and J, Q. Hu, *J. Mater. Chem. A*, 2014, **2**, 4795.

48 M. Huang, Y. X. Zhang, F. Li, L. L. Zhang, Z. Y. Wen and Q. Liu, *J. Power Sources*, 2014, **252**, 98.

49 Y. H. Li, L. J. Cao, L. Qiao, M. Zhou, Y. Yang, P. Xiao and Y. H. Zhang, *J. Mater. Chem. A*, 2014, **2**,6540.

50 M. Kaempgen, C. K. Chan, J. Ma, Y. Cui and G. Gruner, Nano Lett, 2009, **9**, 1872.

51 Q. T. Qu, Y. S. Zhu, X. W. Gao and Y. P. Wu, *Adv. Energy Mater*, 2012, **2**, 950.

52 J. T. Zhang, J. W. Jiang, H. L. Li and X. S. Zhao, *Energy Environ. Sci*, 2011, **4**, 4009.

